AAS 12-218

COMPARISON OF DELAUNAY NORMALIZATION AND THE KRYLOV-BOGOLIUBOV-MITROPOLSKY METHOD

Juan F. San-Juan,* Luis M. López,† David Ortigosa,‡
Martín Lara§ and Paul J. Cefola¶

A scalable second-order analytical orbit propagator program (AOPP) is being carried out. This AOPP combines modern and classical perturbation methods in function of orbit types or the requirements needed for a space mission, such as catalog maintenance operations, long period evolution, and so on. As a first step on the validation and verification of part of our AOPP, we only consider perturbation produced by zonal harmonic coefficients in the Earths gravity potential, so that it is possible to analyze the behavior of the mathematical expression involved in the corresponding analytical theory in depth and determine its limits.

INTRODUCTION

The Iridium/Cosmos satellite collision event in 2009 has demonstrated among other things the necessity of improving orbit prediction methods. In this sense, a scalable second-order analytical orbit propagator program (AOPP) is being carried out. This AOPP combines modern and classical perturbation methods in function of orbit types or the requirements needed for a space mission, such as catalog maintenance operations, long period evolution, and so on.

As a first step on the validation and verification of part of our AOPP, which we will call $\mathrm{PP}_{\mathrm{DN}}^{\mathrm{KB}}$, we only consider perturbation produced by zonal harmonic coefficients in the Earth's gravity potential, such that it is possible to analyze the behavior of the mathematical expression involved in the corresponding analytical theory in depth and determine its limits when classical tasks like critical inclination and small eccentricities and inclination appear.

Most of the analytical theories in the artificial satellite problem start with the elimination of the short period terms.[1,2,3,4] In fact, the most useful AOPP, SGP4[5,6] and PPT2,[7,8] are derived from the Brouwer-Lyddane theory. However, other analytical theories simplify the problem by means of a Lie transform called the elimination of the Parallax.[9] In this work, we explore other alternatives which arise from the elimination of the Parallax. This is based on removing the long period terms by means of the elimination of the Perigee.[10] The transformed Hamiltonian has one degree of freedom and only depends on the radial distance r and $R = \dot{r}$. Finally, the integration of the problem can be made using the classical Delaunay Normalization[11] or by means of the Krylov-Bogoliubov-Mitropolsky method.[12,13]

In this paper, we present part of our AOPP and its validation. It implements a second order closed-form zonal analytical theory, in the cases of J_2–J_4 and J_2–J_{12}, which integrates the problem using the two aforementioned methods. A methodology based on an exploratory data analysis (EDA)[14] is proposed in order to validate both integration methods and determine the values of the TLEs, where these methods are valid in function of the duration of propagation. A TLE space catalog is used as simulated data in order to validate our AOPP. Then we identify the outliers and make a general study of the rest of the TLEs in the case of J_2–J_4.

*Universidad de La Rioja, ES-26004 Logroño, Spain, juanfelix.sanjuan@unirioja.es
†Universidad de La Rioja, ES-26004 Logroño, Spain, luis-maria.lopezo@unirioja.es
‡Universidad de La Rioja, ES-26004 Logroño, Spain, david.ortigosa@unirioja.es
§TENECO, ES-26250 Logroño, Spain, mlara0@gmail.com
¶University at Buffalo, State University of New York, Amherst, New York 14260-440, paulcefo@buffalo.edu

After that we study the TLEs near the critical inclination and analyze the modification implemented in PPT2, HANDE[15] and AOPP[16] in the cases of J_2–J_4 and J_2–J_{12}. Finally we summarize this study.

ANALYTICAL THEORIES

In polar-nodal variables $(r, \theta, \nu, R, \Theta, N)$, the Hamiltonian for an Earth satellite perturbed by zonal harmonic potential terms is given by

$$\mathcal{H} = \frac{1}{2}\left(R^2 + \frac{\Theta^2}{r^2}\right) - \frac{\mu}{r} + \frac{\mu}{r}\sum_{n\geq 2}^{m} J_n \left(\frac{\alpha}{r}\right)^n P_n(\sin i \, \sin\theta), \tag{1}$$

where P_n is the Legendre polynomial of degree n, m is the maximum order of the zonal harmonic perturbation being considered, μ is the gravitational constant, α is the equatorial radius of the planet, and J_n are the zonal harmonic coefficients.

Figure 2 shows the combinations of Lie transforms and classical averaging techniques used to carry out the two analytical theories. Both theories begin by removing the long period terms, due to the argument of the perigee, by combining two Lie transformations, the elimination of the Parallax[9] and the elimination of the Perigee[10] (Lie transforms φ_1 and φ_2 respectively). The transformed Hamiltonian $\mathcal{H}''$, classically known as Radial Intermediary, has one degree of freedom but maintains the short period terms, due to mean anomaly. These two Lie transformations are carried out in a closed form of eccentricity, which leads us to an integrable problem in the variables (r'', R''). Traditionally, to complete the theory and obtain the mean elements like Brouwer,[1] a further reduction is made through Delaunay variables by means of the Delaunay normalization[11] (Lie transform φ_4) which averages the problem over the mean anomaly. However, if the time and variable r'' are replaced by the perturbed true anomaly and the inverse of r'' in the Hamiltonian $\mathcal{H}''$ (φ_3 transform), the equations of motion become a one-dimensional perturbed harmonic oscillator and the Krylov-Bogoliubov-Mitropolsky method[12,13,17,18,19,20,21,22] can also be used to integrate them.

$$\begin{array}{ccc}
\mathcal{H}(r, \theta, _, R, \Theta, N) & & \\
\downarrow \varphi_1 & & \\
\mathcal{H}'(r', \theta', _, R', \Theta', N') & & \\
\downarrow \varphi_2 & & \\
\mathcal{H}''(r'', _, _, R'', \Theta'', N'') \equiv \mathcal{H}''(l'', _, _, L'', G'', H'') & & \\
\varphi_3 \swarrow & & \searrow \varphi_4 \\
\ddot{u} + \omega^2 u = F\left(u, \dot{u}; \epsilon\right) & & \mathcal{H}'''(_, _, _, L''', G''', H''')
\end{array}$$

Figure 1. Two methods to integrate the Radial Intermediary $\mathcal{H}''$. The variable u is related to variable r''.

The analytical theories were carried out maintaining the physical parameters in symbolic form so that they could be valid for any gravity field model. On the other hand, no change of variables has been introduced in the theories so as not to remove any problems generated by small eccentricities and inclinations,[23] as well as the critical inclination, which allows us to evaluate their real impact on the analytical expressions, and so determine the region of the space phase where these problems may appear. However in the case of the critical inclination we will analyze the solution implemented in PPT2.

Table 1 shows the number of terms in Hamiltonians and generators derived from the applications of the previous Lie transforms in the case of $m = 4$ and $m = 12$; that is, the considered perturbations are from J_2 to J_4 in the first case and from J_2 to J_{12} in the second. The direct and inverse transformations[24] of the elimination of the Parallax and Perigee and the Delaunay Normalization may be calculated from their generating functions $\mathcal{W}'$, $\mathcal{W}''$, $\mathcal{W}'''$ respectively. The total number of terms of the series involved in these transformations, in the $m = 4$ and $m = 12$ cases, are $1,330$ and $120,718$ in the elimination of the Parallax, $2,038$ and $1,228,732$ in the elimination of the Perigee and 384 and $3,112$ in the Delaunay Normalization respectively.

Table 1. Number of terms in the initial and transformed Hamiltonians and generators $(m = 4/m = 12)$**.**

Order	Initial	Elimination of the Parallax		Elimination of the Perigee		Delaunay Normalization	
	$\mathcal{H}$	$\mathcal{H}'$	$\mathcal{W}'$	$\mathcal{H}''$	$\mathcal{W}''$	$\mathcal{H}'''$	$\mathcal{W}'''$
0	3	3	–	3	–	1	–
1	3	2	7	2	6/352	2	2
2	9/135	20/504	124/11,121	12/116	33/1,642	21/125	36/140

Table 2 shows the number of terms in the solution using the Krylov-Bogoliubov-Mitropolsky method, whereas the number of terms in Hamilton's equations dl/dt, dg/dt, dh/dt are 24, 23, 16 for $m = 4$ and 122, 121, 98 for $m = 12$.

Table 2. Number of terms for the solution of the differential equation $(m = 4/m = 12)$**.**

$1/r''$	θ''	ν''	R''	Θ''	N''	$\frac{d\delta}{ds}$	$\frac{df_k}{ds}$	Kepler equation
28/297	28/298	17/121	27/297	1	1	0	15/119	108/815

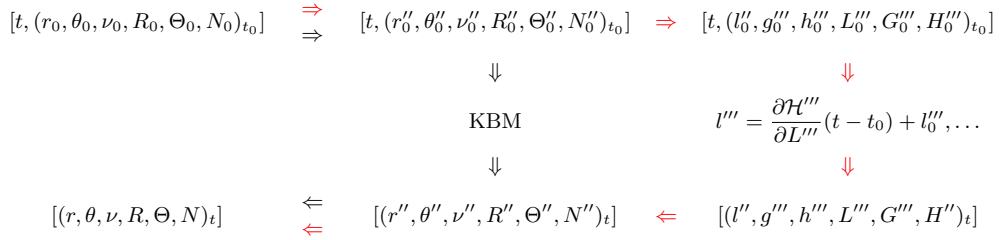

Figure 2. Flowchart of the PP$^{\mathrm{KB}}_{\mathrm{DN}}$ AOPP.

Our AOPP combines these two theories. The analytical expressions and the orbit propagator, coded in C, were performed by the symbolic-numeric environment *MathATESAT*.[25] Figure 2 shows the flowchart of the AOPP orbit propagator. The program begins reading the physical parameters and initial conditions, osculating Keplerian elements or state vector, at the epoch t_0. Next, it transforms the initial conditions in polar-nodal variables, and transports them across the inverse transformations of the elimination of the Parallax and Perigee. At this point the AOPP can use the Krylov-Bogoliubov-Mitropolsky method to provide polar-nodal variables at the epoch t_f, or continue applying the inverse transformations of the Delaunay Normalization, which then evaluate the integrated Hamilton equations and apply the direct transformations of

the Delaunay Normalization. Finally, the direct transformations of the elimination of the Perigee and Parallax are applied, and the osculating Keplerian elements and the state vector are calculated. We use the name KB when the AOPP applies the Krylov-Bogoliubov-Mitropolsky method or DN in the case of the Delaunay Normalization method.

METHODOLOGY

In order to compare the behavior of the Krylov-Bogoliubov-Miropolsky and Delaunay Normalization methods, we make an exploratory data analysis[26] consisting of the study of errors produced by both methods in the zonal case, and in which a space catalog with $14,208$ TLEs is propagated, with the numerical integration of the original problem. The integrator used is a 8th order Runge-Kutta method.[27] Although it is well known that TLEs have been designed to be used in combination with the SGP4 orbit propagator, we consider that a TLE space catalog contains a large and representative number of different types of orbits, which can be considered as a reliable and independent test for our study.

The $14,208$ TLEs were propagated over 7 days with the DN, KB and Runge-Kutta methods. Then the distance, along-track, cross-track, radial and relative errors of the orbital elements were calculated for DN and KB. After that we made an EDA consisting of:

- A graphic study of DN and KB errors using the box and whisker plot. This plot of a data set consists of a box drawn around the median value, where the lower and upper box edges bound the first and third quartiles (Q1 and Q3), respectively. The lower and upper whiskers extending from each bound box are the minimum and maximum values without outliers (circles) and extreme values (asterisks) respectively, whereas $Q_3 + 1.5 * (Q_3 - Q_1)$ and $Q_1 - 1.5 * (Q_3 - Q_1)$ represent the upper and lower limits respectively. We must remark that in this study the extreme values will also be considered as outliers.
- By means of scatter plots to characterize the orbits in which the propagators have a poorer overall performance (greater presence of outliers-those above $Q_3 + 1.5 * (Q_3 - Q_1)$). A study of contingency tables (considering the number of outliers and corresponding orbit as variables) and the calculation of Yule's Q, a measure of the magnitude of association between the two raters, complete the study chart.
- Excluding the atypical, we explore the behavior of the two propagators and the three components of error.
- Finally, we explore the results of the proposed improvements in the two estimates for the orbits near the critical inclination.

Catalog Classification

The orbit data can be separated from the space catalog. The frequency distribution of the semi-major axis a, eccentricity e, inclination i, argument of the node Ω, argument of the perigee ω and the mean anomaly M are presented in Table 3. In the cases of Ω, ω, M, these are in general distributed uniformly between 0° and 360°, but the distribution of a, e, i are not uniform. The values of the semi-major axis are between 1.018543 and 109.2196 Earth Radii in which 50% of the objects have $a < 1.5$ Earth Radii. The eccentricity is between 0.000001 and 0.9203, although almost 60% have $e < 0.01$. The inclination is between 0.00120° and 144.6415°, including data of 270 objects near the critical inclination.

Figure 3 shows a pie chart depicting the distribution of the data following the classification given in.[26] Near circular low Earth, medium Earth, eccentric and low Earth orbits represent 95.6% of the orbit types belonging to the considered catalog. A more detailed description of this classification is shown in Appendix A.

DELAUNAY NORMALIZATION VS KRYLOV-BOGOLIUBOV-MITROPOLSKY (J_2–J_4)

The study began applying the box and whisker plot analysis to the values of the DN and KB distance errors in order to identify potential outliers (see Figure 4). As can be seen, there were no outliers below the lower

Table 3. Frequency distribution of the orbital elements a (Earth Radii), e, i (deg), Ω (deg), ω (deg), M (deg).

a	$(1, 1.05)$	$[1.05, 1.10)$	$[1.10, 1.15)$	$[1.15, 1.20)$	$[1.20, 1.25)$	$[1.25, 1.30)$	≥ 1.30
Num.	37	976	6413	1957	1540	273	3012
%	0.3	6.9	45.1	13.8	10.8	1.9	21.2
e	$[0, 0.0015)$	$[0.0015, 0.003)$	$[0.003, 0.006)$	$[0.006, 0.01)$	$[0.01, 0.02)$	$[0.02, 0.05)$	$[0.05, 1]$
Num.	2297	1679	2108	1794	2326	1685	2317
%	16.2	11.8	14.8	12.6	16.4	11.9	16.3
i	$[0, 20)$	$[20, 40)$	$[40, 60)$	$[60, 80)$	$[80, 100)$	$[100, 120)$	$[120, 180)$
Num.	1561	553	456	4062	6711	833	30
%	11.0	3.9	3.2	28.6	47.2	5.9	0.2
Ω	$[0, 60)$	$[60, 120)$	$[120, 180)$	$[180, 240)$	$[240, 300)$	$[300, 360)$	
Num.	3138	2961	2174	1644	1708	2581	
%	22.1	20.8	15.3	11.6	12.0	18.2	
ω	$[0, 60)$	$[60, 120)$	$[120, 180)$	$[180, 240)$	$[240, 300)$	$[300, 360)$	
Num.	2134	2574	2481	2438	2461	2118	
%	15.0	18.1	17.5	17.2	17.3	14.9	
M	$[0, 60)$	$[60, 120)$	$[120, 180)$	$[180, 240)$	$[240, 300)$	$[300, 360)$	
Num.	2460	2267	2309	2261	2404	2505	
%	17.3	16.0	16.3	15.9	16.9	17.6	

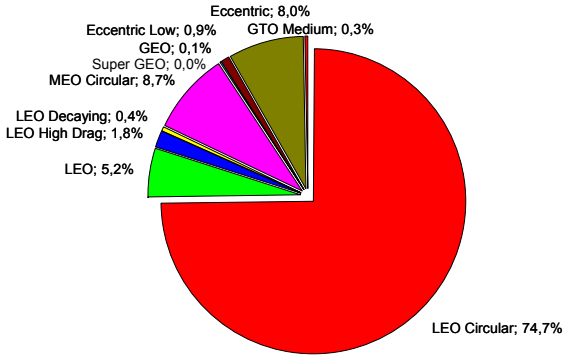

Figure 3. Catalog classification.

whisker limit, but if there had been any they would have represented very good behavior for the analytical methods in the corresponding TLE. Outliers larger than 5 m have not been included in this graphic. The values of the median, minimum, maximum, first and third quartiles and the upper whisker limit are shown in Table 4.

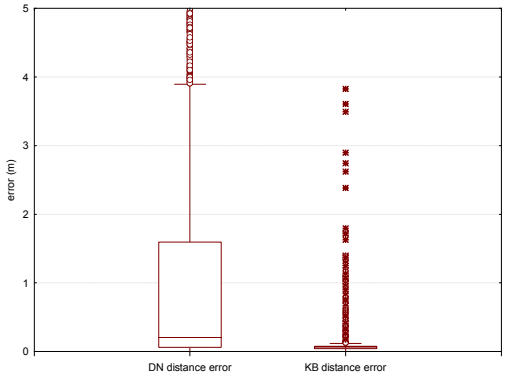

Figure 4. Box and whisker plot analysis of the DN and KB distance errors.

Table 4. Statistical parameters DN and KB distance errors (m).

Error	Median	Minimum	Maximum	Q_1	Q_3	$Q_3 + 1.5 * (Q_3 - Q_1)$
DN	0.202258	0.000002	83620353	0.061806	1.595556	3.90
KB	0.063508	0.000001	83620353	0.042548	0.074012	0.12

The number of outliers detected in the DN and KB cases are $2,662$ and 147 respectively, of which only 55 are common. DN outliers represent 33% of the TLEs whose eccentricity is less than 0.01, thus this strong association is confirmed by Yule's Q (0.97), and when the distance error is obtained from TLEs with $e \geq 0.01$ and near the critical inclination, between $62.5°$ and $64.5°$, outliers represent 47% of the corresponding TLEs, which in this case Yule's Q (0.997) also indicates a very strong association. For KB, 50% of outliers also correspond to TLEs near the critical inclination, between $62.5°$ and $64.5°$, with Yule's Q =0.998, whilst 12 of the remaining 16 outliers correspond to TLEs with inclinations of less than $1.5°$ and $e > 0.5$ and where Yule's Q is 0.985. We must remark that the maximum distance error in these cases is less than 6 m. Figure 5 shows the distribution of the eccentricity vs. inclination of the full TLE catalog and the TLEs which correspond to DN and KB distance error outliers.

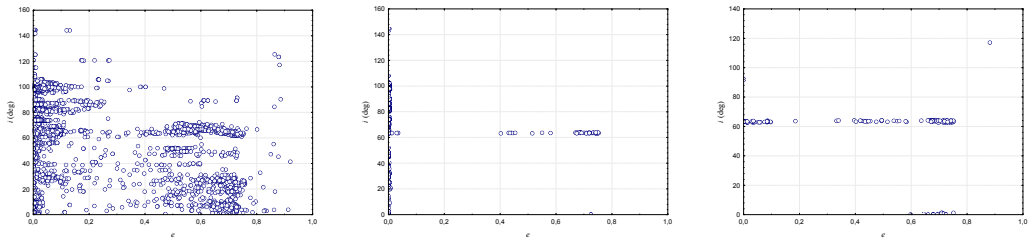

(a) Full catalog. (b) DN outliers. (c) KB outliers.

Figure 5. The distribution of the eccentricity vs inclination.

Then we will study the behavior of the Delaunay Normalization and Krylov-Bogoliubov-Mitropolsky methods starting from distance, along-track, cross-track and radial errors.

The histogram of DN distance error is shown in Figure 6 (a). We should mention that the lack of robustness of estimates is due to the asymmetry on the right of the histogram. This asymmetry corresponds to TLEs with small eccentricity, $e < 0.01$, and near the critical inclination. Figure 6 (b) shows a box and whisker plot of the distance, along-track, cross-track and radial errors without upper outliers. These data have been classified in three sets: $e < 0.01$, $e \geq 0.01$ and $62.5^\circ < i < 64.5^\circ$, and any other data. The most influential errors for TLEs with $e < 0.01$ are found in the along-track and radial components, whereas for TLEs with $e \geq 0.01$ and $62.5^\circ < i < 64.5^\circ$ the worst error behavior was found to be in the cross-track component.

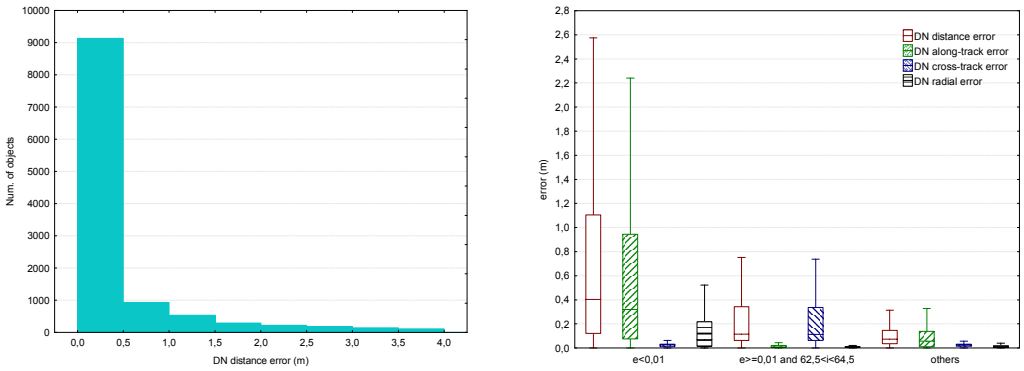

(a) DN distance error histogram.

(b) Distance, along-track, cross-track and radial errors.

Figure 6. Delaunay Normalization method.

The histogram of KB distance error exhibits fairly symmetric behavior, as can be seen in Figure 7 (a). We must bear in mind the robustness of estimates. Figure 7 (b) shows a box and whisker plot of the distance, along-track, cross-track and radial errors without upper outliers. These data have been classified as mentioned in the previous paragraph. However in this case the most influential errors for TLEs with $e < 0.01$ are found in the along-track and cross-track components, whereas for TLEs with $e \geq 0.01$ and $62.5^\circ < i < 64.5^\circ$ the worst error behavior was found to be in the cross-track component as in the DN case. Note the scarce influence of radial error in the three cases.

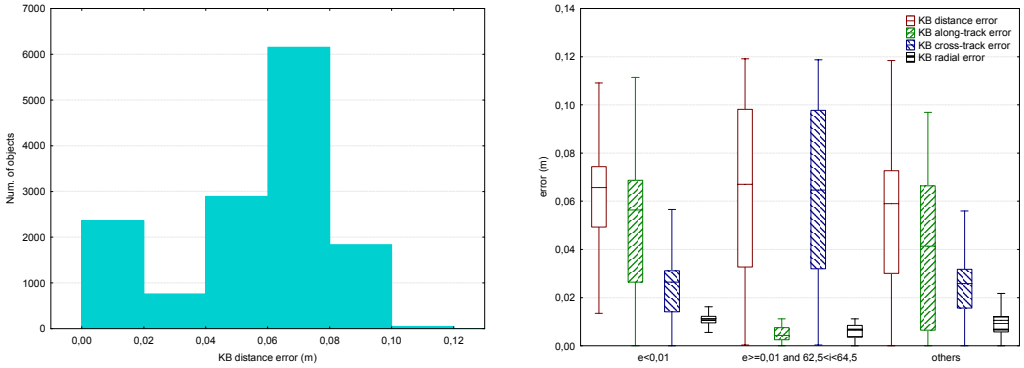

(a) KB distance error histogram.

(b) Distance, along-track, cross-track and radial errors.

Figure 7. Krylov-Bogoliubov-Mitropolsky method.

Figure 8 shows a box and whisker plot analysis for DN and KB distance errors taking into account the classification suggested in.[26] The number of data in each type of orbits is not uniform; for further details

see Table 14 in Appendix A. Upper and lower outliers of less than 3.9 m are taken into account in this plot. Figure 8 (b) shows lower outliers for LEO Circular category ($n > 4$, $a_p > 300$, $e \leq 0.05$) in which the Krylov-Bogoliubov-Mitropolsky method provides good orbit determination compared with all other TLEs in this category.

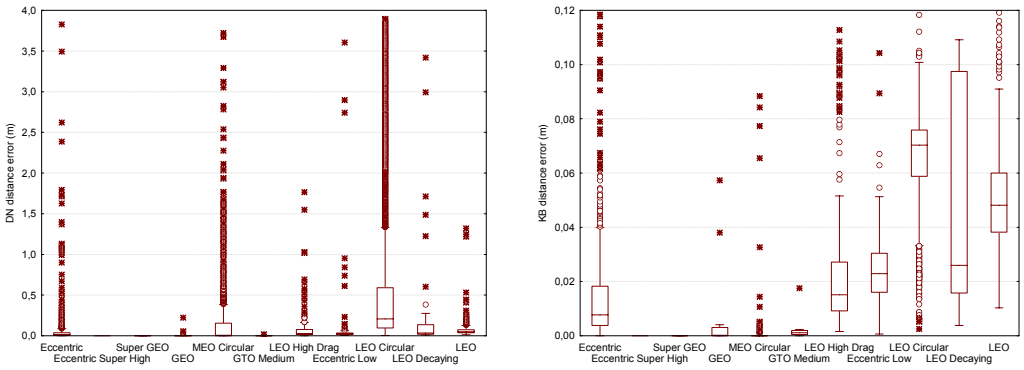

(a) DN distance errors.

(b) KB distance errors.

Figure 8. Box and whisker plot analysis for DN and KB distance errors taking into account the classification suggested in.[26]

The previous analysis shows the robustness of estimations produced by the Krylov-Bogoliubov-Mitropolsky method vs. the Delaunay Normalization. In fact, the behavior of the Krylov-Bogoliubov-Mitropolsky method is better than the Delaunay Normalization in 87% of the cases, where the mean value is only 0.0083 m; for further details see Table 5.

Table 5. Comparison of the Krylov-Bogoliubov-Mitropolsky and the Delaunay Normalization.

Orbit Class	Number of Objects	% KB better than DN
LEO Circular	$10,612$	92%
LEO	733	60%
LEO High Drag	250	74%
LEO Decaying	60	75%
MEO Circular	$1,231$	97%
GEO	16	69%
Super GEO	4	100%
Eccentric Low	128	48%
Eccentric	$1,131$	53%
Eccentric Super High	1	100%
GTO Medium	42	52%
Total Catalog	$14,208$	87%

In particular, the worst behavior of the Delaunay Normalization is found in the $e < 0.01$ category. Table 6 shows the mean and median values for DN and KB a, e, i, g, l errors ($e < 0.01$). It is noteworthy that the relative semi-major axis error is only slightly better in the DN than KB cases, 0.0035 m vs 0.0045 m in mean values respectively. Eccentricity, argument of the perigee and mean anomaly errors are much better in the KB than DN cases, whereas the behavior of the inclination and the argument of the node errors are similar in DN and KB. Figure 9 shows box and whisker plot analysis, without outliers, for semi-major axis, eccentricity, argument of the perigee and mean anomaly errors in this category. The worst eccentricity and mean anomaly

determinations using the Delaunay Normalization method, in this case, explains the influence of the radial error over the cross-track error (Figure 9 (b) and (d)).

Table 6. Statistical parameters DN and KB orbital elements errors ($e < 0.01$).

	DN Mean	DN Median	KB Mean	KB Median
a	0.00350136090	0.00305716275	0.00457735125	0.00474952776
e	0.00000002971	0.00000001514	0.00000000164	0.00000000141
i	0.00000000005	0.00000000006	0.00000000005	0.00000000006
g	0.00002127543	0.00000425125	0.00000048432	0.00000030621
l	0.00002127544	0.00000424892	0.00000048335	0.00000030486

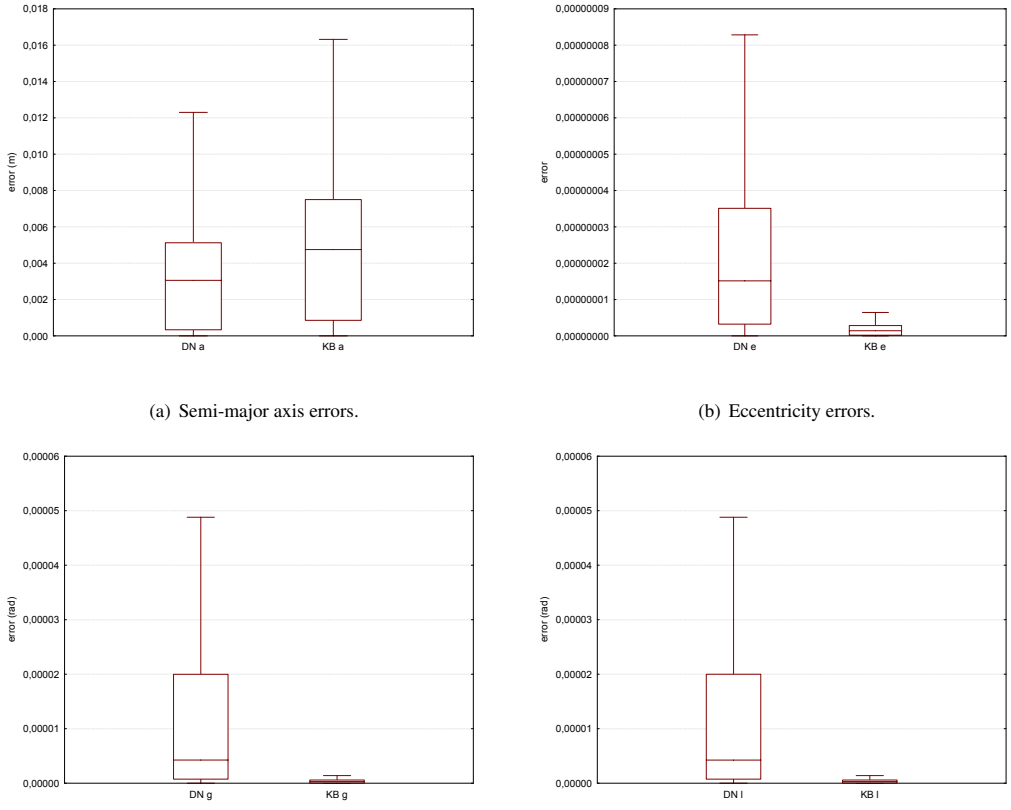

(a) Semi-major axis errors.

(b) Eccentricity errors.

(c) Argument of the perigee errors.

(d) Mean anomaly errors.

Figure 9. Box and whisker plots for DN and KB orbital element errors.

We want to finish this section analyzing some of the KB outliers. In particular, those corresponding to TLEs with $e > 0.5$ and $i < 1.5°$. The two methods exhibit similar behavior, but on studying this set of outlier values the KB is slightly better then DN, 0.12 m vs $0,14$ m in mean values respectively, as can be seen in Figure 10.

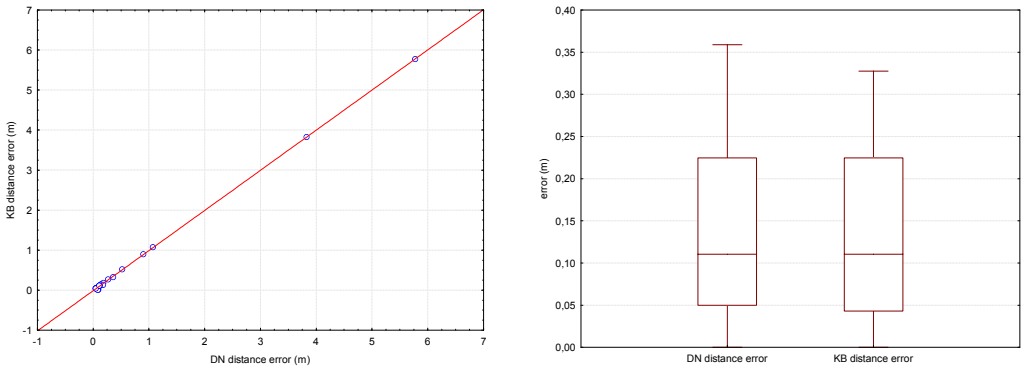

(a) DN vs KB distance error.

(b) Box and whisker plot.

Figure 10. KB outliers ($e > 0.5$ and $i < 1.5°$).

OUTLIERS NEAR CRITICAL INCLINATION

The number of TLEs in the space catalog considered in this study are 270, between $62.5°$ and $64.5°$, of which 58 have eccentricity of less than 0.01, and are not taken into account with the Delaunay Normalization method. Remember that this singularity is directly related to the denominator $1 - 5\cos^2 i''$, which appears in the direct and inverse transformations of the elimination of the Perigee. We must point out that this Lie transform is not valid in the neighborhood of $i = 63.45°$.

In order to reduce the impact of this singularity over this transform, we replace the terms $1/x$ by

$$T2 = \frac{1 - e^{\beta x^2}}{x} = \beta x \sum_{n=0}^{12} (-1)^n \frac{\beta^n x^{2n}}{(n+1)!} \prod_{m=0}^{10} \left(1 + e^{-2^m \beta x^2}\right),$$

where $x = 1 - 5\cos^2 i''$ and $\beta = 100/2^{11}$. This solution has been implemented in other analytical orbit propagator programs (PPT2, HANDE and AOPP). DN2 and KB2 will make reference to the errors obtained with our modified analytical orbit propagator program. We must mention that this modified propagator does not integrate the Hamiltonian (1) exactly but is an approximation which must be identified and its space phase need to be characterized. Here we present the preliminary numerical analysis. The first subsection studies the the behavior of the DN2 and KB2 near the critical inclination in the case of J_2–J_4 perturbations, while in the second we only analyze the Krylov-Bogoliubov behavior for J_2–J_{12} perturbations.

J_2–J_4 perturbations

The data considered in this study correspond to TLEs with $e \geq 0.01$ and $i \in (62.5°, 64.5°)$. Several of these TLEs have distance errors of more than 10^7 m, and overflow values are obtained in two cases. Table 7 shows through statistical parameters that the behavior of DN and KB distance errors is similar for each TLE.

Table 7. Statistical parameters in DN and KB distance errors (m).

	Median	Minimum	Maximum	Q_1	Q_3	$Q_3 + 1.5 * (Q_3 - Q_1)$
DN	0.174277	0.000313	83620353	0.083627	2.089765	5.10
KB	0.173565	0.000313	83620353	0.082587	2.089800	5.10

Table 8 shows the values of the median, minimum, maximum, first and third quartiles and the upper whisker limit in the cases of DN2 and KB2 distance errors for all TLEs, including the two data which generate

overflows. Figure 11 shows that the behavior in both cases is very similar. The maximum error is 133 m. A few outlier values, which in most cases are inferior to 40 m, of which 75% are less than 18.6 m, and of these half are less than 4.75 m, can be observed

Table 8. Statistical parameters in DN2 and KB2 distance errors (m).

	Median	Minimum	Maximum	Q_1	Q_3	$Q_3 + 1.5 * (Q_3 - Q_1)$
DN2	4.735359	0.0000134	133.4178	0.818214	18.63646	45.36
KB2	4.735458	0.0000159	133.4178	0.816421	18.63655	45.37

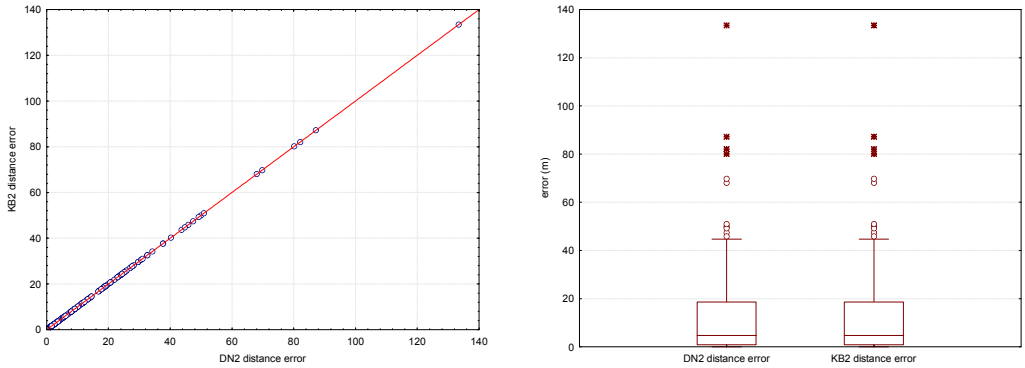

(a) DN2 vs KB2 distance error.

(b) Box and whisker plot of the DN2 vs KB2 distance error.

Figure 11. Modified direct and inverse transformations of the elimination of the Perigee.

Table 9 shows that robustness was not obtained from a general improvement of estimates; in fact, in 75% of the cases, the behavior of both estimators was worse, but original outlier estimates were improved. 165 estimates obtained by the modified models in the non-outlier cases were worse, between 0.37 m and 13.28 m in mean values, while the remaining 47 outliers and the two overflows were reduced to 8.2 m in mean value.

Table 9. Statistical parameters in DN/DN2 and KB/KB2 distance errors (m).

	Mean	Median	Minimum	Maximum
DN(non-outliers)/DN2	0.3742/13.275	0.1139/6.0134	0.000313/0.000134	3.6050/133.4178
KB(non-outliers)/KB2	0.3734/13.271	0.1118/6.0146	0.000313/0.000159	3.6049/133.4178
DN(outliers)/DN2	4547873/8.2295	119.45/3.0804	5.1048/0.00131	83620353/80.1421
KB(outliers)/KB2	4547873/8.2285	119.45/3.0803	5.1049/0.00135	83620353/80.1422

Figure 12 shows the box and whisker plot of the DN2 and KB2 distance errors; in this case the cross-track error is also the most influential, as was seen in the previous general study.

J_2–J_{12} perturbations

We consider the same previous 270 TLEs with $i \in (62.5°, 64.5°)$. Several of these TLEs have distance errors of more than 10^8 m, and overflow values were obtained in ten cases. Table 10 shows the values of the median, minimum, maximum, first and third quartiles and the upper whisker limit in the case of the KBJ12 distance error. Figure 13 (a) shows a box and whisker plot of the KBJ12 distance error in which only 5 of 56 outliers were included.

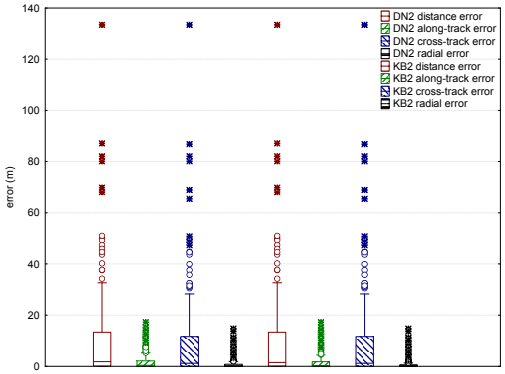

Figure 12. DN2 and KB2 distance errors.

Table 10. Statistical parameters KBJ12 distance error (m).

	Median	Minimum	Maximum	Q_1	Q_3	$Q_3 + 1.5 * (Q_3 - Q_1)$
KBJ12	859.8631	0.009345	133147992	9.32829	8070.470	20162.18

Table 11 shows the statistical parameters for KBJ12_2 distance error for all TLEs including the ten data which generate overflows. Figure 13 (b) shows a box and whisker plot for KBJ12_2 distance error; as can be observed there are no outlier values.

Table 11. Statistical parameters KBJ12_2 distance error (m).

	Median	Minimum	Maximum	Q_1	Q_3	$Q_3 + 1.5 * (Q_3 - Q_1)$
KBJ12_2	634.4462	0.249139	2247.630	310.6079	1127.350	2352.4631

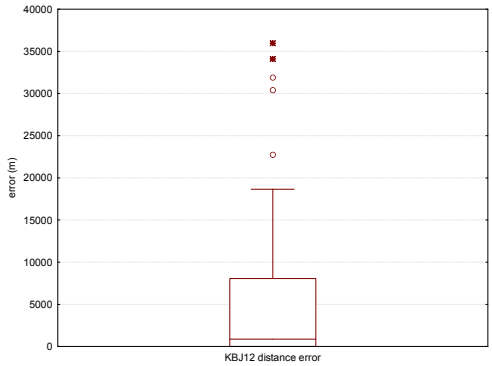

(a) KBJ12 distance error.

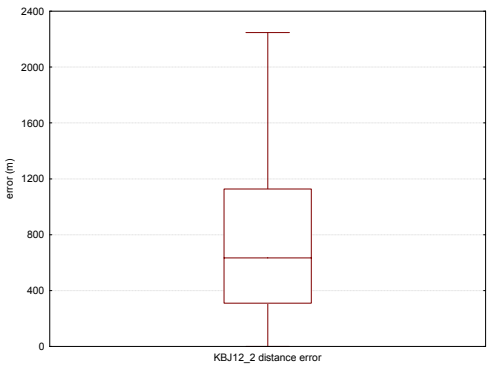

(b) KBJ12_2 distance error.

Figure 13. Box and whisker plot of the KBJ12 and KBJ12_2 distance errors.

Although the ephemeris generated by the second-order theory in the J_2–J_4 case provides good accuracy, this becomes worse when the number of zonal harmonics increases. The same precision is only obtained

if third-order effects are included. However the behavior of the modified second-order direct and inverse transformations of the elimination of the perigee in J_2–J_{12} is, in general, better than in J_2–J_4. The estimation in 142 cases, including the ten overflow values, is better in KBJ12_2, being 967 m in mean value, but is worse in 128 cases, between 184 m and 503 m in mean values, as can be seen in Table 13. Another difference with J_2–J_4 is that in J_2–J_{12} the main error is obtained in the along-track component, as can be seen in Figure 14.

Table 12. Statistical parameters KBJ12 and KBJ12_2 distance errors (m).

Model	Num. of data	Mean	Median	Minimum	Maximum
KBJ12	128	184.3634	6.6210	0.009345	1720.197
KBJ12_2	128	503.3113	311.52	0.249139	1796.142
KBJ12	142	5671673	7939.072	166.2859	133147992
KBJ12_2	142	967	763.488	2.44315	2248

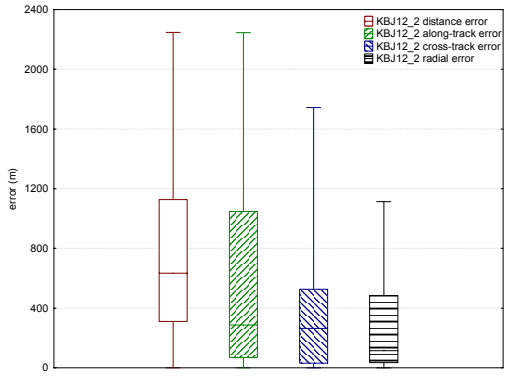

Figure 14. Box and whisker plot of the KBJ12_2 distance error.

Finally a detailed study is presented to determine the range of influence of the critical inclination. As might be expected, the behavior of the analytical theory becomes worse when we are near inclinations 63.43494882292° or 116.5650511770779°. We restrict our study to the interval $(62.5^\circ, 64.5^\circ)$, which has been divided into five subintervals. Figure 15 shows the distribution of the KB12 distance error in the five subintervals. This distribution is similar in the case of J_2–J_4 perturbations. As can be observed, in the interval $[63.33^\circ, 63.66^\circ)$ the errors produced by the analytical theory are greater, whereas in the rest of the intervals other large errors can be found.

Figure 16 (a) compares the KB12 vs KB12_2 distance errors, whilst Figure 16 (b) shows the box and whisker plot analysis for KB12_2 distance errors at each subinterval.

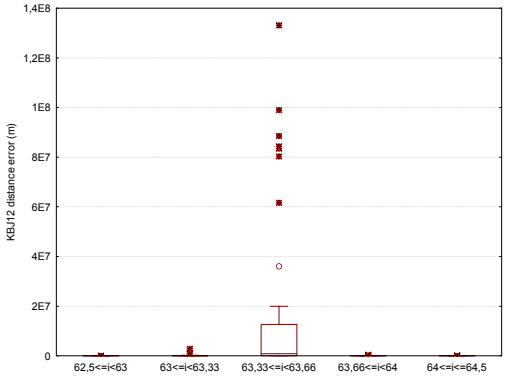

Figure 15. Box and whisker plot of the KB12 distance error.

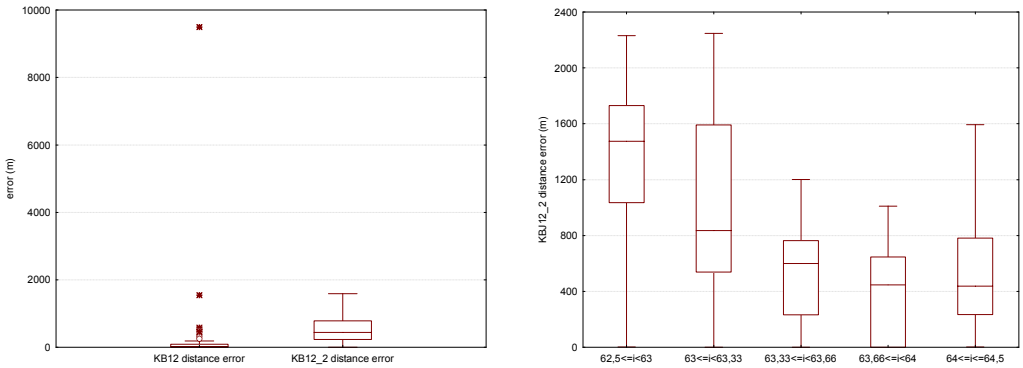

(a) KB12 vs KB12_2 distance errors.

(b) KB12_2 distance errors in the subintervals.

Figure 16. Box and whisker plots.

Table 13. Statistical parameters KBJ12 and KBJ12_2 distance errors (m).

i	Model	Num. of data	Median	Minimum	Maximum
$62.5° \leq i < 63°$	KBJ12	64	1651	0.027	35992
	KBJ12_2	64	1474	1.93	2231
$63° \leq i < 63.33°$	KBJ12	31	56799	0.015	2.8×10^6
	KBJ12_2	31	836	0.85	2247
$63.33° \leq i < 63.66°$	KBJ12	49	8×10^8	0.014	1.3×10^8
	KBJ12_2	49	600	0.25	1200
$63.66° \leq i < 64°$	KBJ12	71	400	0.015	4.3×10^5
	KBJ12_2	71	446	0.5	1882
$64° \leq i < 64.5°$	KBJ12	55	20.38	0.009	9495
	KBJ12_2	55	438	2.13	1593

CONCLUSION AND FUTURE WORK

A scalable closed-form analytical orbit propagator program is being developed. In this paper only zonal harmonic perturbation is considered. This perturbation can be handled by means of two analytical theories. Both are derived after removing the long-period perturbation terms due to the argument of the perigee. The first removes the short-period terms due to the mean anomaly, using the classical Delaunay Normalization, and then the transformed Hamiltonian is trivially integrated. We remark that Delaunay variables are used here. The second removes the short period terms by means of the Krylov-Bogoliubov-Mitropolsky method. This process is formulated in polar-nodal variables. In order to validate both models a TLE space catalog is used. Although this input is only valid for SGP4, it can be considered a reliable set of initial conditions to validate our propagator. These data have been classified in three sets ($e < 0.01$, $e \geq 0.01$ and $62.5^\circ < i < 64.5^\circ$, and any other data) and an exploratory data analysis is applied to analyze the errors produced by our propagator in the ND and KB cases, when these are compared with the numerical integration of the original problem.

The number of outliers are $2,662$ and 147 in the ND and KB cases respectively, of which only 55 are common when the TLEs are propagated over 7 days. The DN outliers are located in TLEs with $e < 0.01$ and $e \geq 0.01$ and $62.5^\circ < i < 64.5^\circ$, whereas for KB the outliers appear near the critical inclination and in $e > 0.5$ and $i < 1.5^\circ$, which are relative outliers with an error of less than 8 m. The critical inclination is handled using the approximation implemented in PPT2, HANDE and AOPP in the cases $m = 4$ and $m = 12$. Preliminary numerical analysis seems to be very promising in the inclination interval $(62.5^\circ, 64.5^\circ)$. In general our conclusion is that KB is clearly more robust than DN in 87% of the study cases over 7 days, and whenever DN is better than KB, it is only slightly better. In all cases the behavior of the polar-nodal variables is excellent and does not present any problem, including $e < 0.01$.

Currently, we are analyzing the behavior of the theories for propagation of over 30 days. On the other hand, the orbit classification proposed in[26] shows that it is necessary to extend this study with more TLEs or fictitious initial conditions in order to explore further regions of values in depth. We will replace Delaunay variables by nonsingular variables. We generate third order analytical theories for $m > 4$ perturbation. We will also analyze how using the polynomial $T2$ instead of $1/(1 - 5\cos i'')$ may modify the original Hamiltonian and what its corresponding phase space may be. Tesseral influence will be the next perturbation to be included in $\mathrm{PP}_{\mathrm{DN}}^{\mathrm{KB}}$.

ACKNOWLEDGMENT

Part of this research has been supported by the Government of Spain (Projects AYA 2009-11896, AYA 2010-18796 and grant Gobierno de La Rioja Fomenta 2010/16).

APPENDIX A: CATALOG CLASSIFICATION

Table 14 show 13 orbit classes introduced in,[26] which categorizes large amounts of data, where

- LEO Circular indicate near circular low Earth orbits.
- GEO are geosynchronous orbits.
  - Super GEO are super-synchronous orbits (i.e., orbits above the geosynchronous belt).
- Eccentric are eccentric orbits that do not cross the geo belt.
- GTO refers to an orbit that crosses the geosynchronous belt.
  - GTO High refers to an orbit much higher than the geosynchronous belt.
  - GTO Low refers to an orbit that passes through low Earth orbit.
  - GTO Medium refers to an orbit passing through medium altitudes (between LEO and GEO).

Table 14. Catalog Classification. n = Mean Motion (revs/day), e = Eccentricity, a = Semi-major Axis (Earth Radii), r_a = Radius of Apogee (Earth Radii), r_p = Radius of Perigee (Earth Radii), a_p = Perigee Altitude (km).

Orbit Class	Definition	Number of Objects ($i \leq 63^\circ$ and $i \geq 64^\circ$)
LEO Circular	$n > 4$, $a_p > 300$, $e \leq 0.05$	$10,612$
LEO	$n > 4$, $0.05 < e < 0.2$	733
LEO High Drag	$200 \leq a_p < 300$	250
LEO Decaying	$a_p \leq 200$	60
MEO Circular	$n \leq 4$, $e < 0.05$	$1,231$
GEO	$n \leq 1.1$, $a < 6.8$	16
Super GEO	$a \geq 6.8$, $e < 0.2$	4
Eccentric Low	$n > 4$, $0.2 \leq e < 0.5$	128
Eccentric	$e \geq 0.5$	$1,131$
Eccentric Super High	$a \geq 6.8$, $e \geq 0.2$	1
GTO Low	$r_p \leq 2.0$, $r_a \geq 6.0$, $e \geq 0.5$, $\|\|i\|\| \leq 10$	0
GTO Medium	$n \leq 4$, $0.1 \leq e < 0.5$	42
GTO High	$r_a \geq 7.0$, $e \geq 0.5$	0
Total:		$14,208$

REFERENCES

[1] Brouwer, D., "Solution of the Problem of Artificial Satellite Theory Without Drag," *Astronomical Journal*, Vol. 64, 1959, pp. 379–397.

[2] Kozai, Y., "Second-order solution of artificial satellite theory without air drag," *Astronomical Journal*, Vol. 67, 1962, pp. 446–461.

[3] Aksnes, K., "A Second-Order Artificial Satellite Theory Based on an Intermediate Orbit," *Astronomical Journal*, Vol. 75, 1970, pp. 1066–1076.

[4] Kinoshita, H., "Third-order solution of an artificial satellite theory," Smithsonian Astrophysical Observatory, Special Report No. 379, Cambridge, Massachusetts, 1977.

[5] Hoots, F. R., and Roehrich, R. L., "Spacetrack Report #3: Models for Propagation of the NORAD Element Sets," U.S. Air Force Aerospace Defense Command, Colorado Springs, CO, 1980.

[6] Vallado, D. A., Crawford, P. Hujsak, R. and Kelso, T. S., "Revisiting Spacetrack Report #3,"AIAA/AAS Astrodynamics Specialist Conference, Keystone, CO, 2006.

[7] "PPT2: The NAVSPASUR Model of Satellite Motion,"NAVSPASUR Report 92-01, July 1992. Available from Commander, NAVSPACECOM, 5280 Fourth Street, Dahlgren, VA 22448-5300; attention: Logistics and Information Systems Division (Mail Code N4/6).

[8] Cefola, P. J., and Fonte, D. J., "Extension of the Naval Space Command Satellite Theory to include a General Tesseral m- daily Model," Paper AIAA-96-3606 presented at the AIAA/ AAS Astrodynamics Conference. San Diego, CA, 1996.

[9] Deprit, A., "The Elimination of the Parallax in Satellite Theory," *Celestial Mechanics and Dynamical Astronomy*, Vol. 24, No. 2, 1981, pp. 111–153.

[10] Alfriend, K. T. and Coffey, S. L., "Elimination of the perigee in the satellite problem," *Celestial Mechanics and Dynamical Astronomy*, Vol. 32, No. 2, 1984, pp. 163–172.

[11] Deprit, A., "Delaunay normalisations," *Celestial Mechanics and Dynamical Astronomy*, Vol. 26, No. 1, 1982, pp. 9–21.

[12] Krylov, N. and Bogoliubov, N. N., "Introduction to Nonlinear Mechanics," Princeton University Press, Princeton, New Jersey, 1947.

[13] Bogoliubov, N. N. and Mitropolsky, Y. A., "Asymptotic method in the theory of non-linear oscillations," Gordon and Breach, New York, 1961.

[14] Tukey, J. W., "Exploratory data analysis," Addison Wesley Publishing, Reading,1977.

[15] Hoots, F. R. and France, R. G., "An analytic satellite theory using gravity and a dynamic atmosphere," *Celestial Mechanics*, Vol. 40, No. 1, 1987, pp. 1–18.

[16] Coffey, S. L., Neal, H. L., Segerman, A. M. and Travisano, J. J., "An Analytic Orbit Propagation Program for Satellite Catalog Maintenance," paper AAS 1995-426, presented at AAS/AIAA Astrodynamics Specialist Conference, Halifax, Nova Scotia, Canada, 1995.

[17] Calvo, M., "Aplicación del método de promedios al estudio del movimiento de satélites artificiales," Ph.D. Thesis, University of Zaragoza, 1971.

[18] Caballero, J. A., "Movimiento de un satélite artificial bajo la acción gravitatoria terresre. Teoría de segundo orden en variables de Hill," Ph.D. Thesis, University of Zaragoza, 1975.

[19] Sein–Echaluce, M., "Estudio comparativo de intermediarios radiales y su aplicación a la teoría del satélite artificial zonal," Ph.D. Thesis, University of Zaragoza, 1986.

[20] Abad, A., San-Juan, J.F. and Gavín, A., "Short term evolution of artificial satellites," *Celestial Mechanics and Dynamical Astronomy*, Vol. 79, No. 4, 2001, pp. 277–296.

[21] San-Juan, J. F. and Serrano, S., "Application of the Z6PPKB ATESAT–model to compute the orbit of an artificial satellite around Mars," Centre National d'Etudes Spatiales, Technical Report No. DTS/MPI/MS/MN/2000-057, Toulouse, Francia, 2000.

[22] San-Juan, J. F., Gavín, A, López, L. M. and López, R., "PPKBZ9$^{\mathcal{A},\mathcal{SA}}$ two orbit propagators based on an analytical theory," accepted for publication in the Journal of the Astronautical Sciences.

[23] Lyddane, R. H., "Small eccentricities or inclinations in the Brouwer theory of the artificial satellite," *Astronomical Journal*, Vol. 68, 1963, pp. 555–558.

[24] Kamel, A. A., "Perturbation methods in the theory of nonlinear oscillations," *Celestial Mechanics and Dynamical Astronomy*, Vol. 3, No. 1, 1970, pp. 1, 90–106.

[25] San-Juan, J. F., López, L. M. and López, R., "MathATESAT: A Symbolic-Numeric Environment in Astrodynamics and Celestial Mechanics," *Lecture Notes in Computer Science*, Vol. 6783, 2011, pp. 436-449.

[26] Tanygin, S., and Coppola, V., "Survey of Orbit Non-Linearity Effects in the Space Catalog," paper AAS 2010-202, presented at AAS/AIAA Space Flight Mechanics Meeting, San Diego, 2010.

[27] Dormand, J. R. and Prince, P. J., "Practical Runge-Kutta Processes," *SIAM Journal on Scientific and Statistical Computing,* Vol 10, No. 5, 1989, pp. 977–989.